Rapid Communications

Transport of intense particle beams in large-scale plasmas

B. Z. Chen,[1,2] D. Wu,[2,*] J. R. Ren,[1] D. H. H. Hoffmann,[1] and Y. T. Zhao[1,†]

[1]*MOE Key Laboratory for Nonequilibrium Synthesis and Modulation of Condensed Matter, School of Science, Xi'an Jiaotong University, Xi'an 710049, China*

[2]*Institute for Fusion Theory and Simulation, Department of Physics, Zhejiang University, Hangzhou 310058, China*

(Received 9 September 2019; revised manuscript received 12 March 2020; accepted 30 April 2020; published 26 May 2020)

Transport of particle beams in plasmas is widely employed in fundamental research, industry, and medicine. Due to the high inertia of ion beams, their transport in plasmas is usually assumed to be stable. Here we report the focusing and flapping of intense slab proton beams transporting through large-scale plasmas by using a recently developed kinetic particle-in-cell simulation code. The beam self-focusing effect in the simulation is prominent and agrees well with previous experiments and theories. Moreover, the beam can curve and flap like turbulence as the beam density increases. Simulation and analysis indicate that the self-generated magnetic fields, produced by movement of collisional plasmas, are the dominant driver of such behaviors. By analyzing the spatial growth rate of magnetic energy and energy deposition of injected proton beams, it is found that the focusing and flapping are significantly determined by the injected beam densities and energies. In addition, a remarkable nonlinear beam energy loss is observed. Our research might find application in inertial confinement fusion and also might be of interest to the laboratory astrophysics community.

DOI: 10.1103/PhysRevE.101.051203

I. INTRODUCTION

The transport of particle beams in plasmas is of great interest in fundamental research and applications, such as accelerator physics [1,2], high-energy density physics [3–6], and inertial confinement fusion (ICF) [7,8] as well as astrophysical shocks [9,10] and cosmic rays [11,12]. Beam-plasma instabilities often play an important role in this research. For specific applications, they certainly should be controlled, for example, by fast ignition for ICF [13] and plasma wake-field acceleration [14–17], while for some studies, instabilities by themselves are worthy of research efforts. For instance, beam focusing can be applied to a plasma lens [18–28]. A proton beam of a cyclotron was focused for the first time by a plasma lens by Panofsky and Baker [18]. The first heavy-ion beam focusing experiment was carried out by Boggasch *et al.* [19]. Furthermore, a plasma lens for the heavy-ion accelerator was investigated by Basko *et al.* [21]. There are also beam self-focusing experiments by Gilson and co-workers [23,24] and theoretical analyses and numerical simulations by Kaganovich and co-workers [25–28] and Hu *et al.* [29]. Additionally, in astrophysics, supersonic flows generate electromagnetic fields through instabilities and then particles can be accelerated to high-energy cosmic rays [30,31].

Numerical simulation is a common method for particle interaction research. For ICF or plasma astrophysics, the spatial and temporal scales of simulations are usually very large. Fluid approaches [32–36] have dominated the research for a long time, but microkinetic processes, like particle acceleration or deceleration and kinetic instabilities, have not been considered. In recent years, there has been a tendency to treat plasma with kinetic methods rather than considering it from a fluid perspective. The particle-in-cell (PIC) simulation method [37–41] has been established as a state-of-the-art method in kinetic plasma physics. It is a compromise between direct particle interaction (such as the molecular dynamics method [42,43] and the N-body method [44,45]) and the Vlasov method [46–48]. It proves to be a valuable tool in studying many astrophysical phenomena from first principles [49].

However, the PIC method still faces challenges. When the densities of particle beams and plasmas differ by orders of magnitude, for instance, the beam density is three orders of magnitude lower than the plasma density [50] and direct PIC simulation of the beam-plasma interaction becomes very difficult. When spatial and temporal scales are normalized by low-density particle beams, there will be significant numerical self-heating and instabilities in overdense plasmas; when normalized by high-density plasmas, the simulation demands dramatically massive simulation grids and time steps, which is currently an unaffordable task for state-of-the-art supercomputers. Since this interaction between ion beams and comparatively-high-density plasmas widely exists in astrophysical plasmas [9–12] and ICF [7,51], a competent kinetic method that can be applied in this situation is of great importance. Recently, an advanced numerical code, LAPINS, was proposed which combines the PIC method with a reduced model of high-density plasma based on Ohm's law [52–56]. This code is able to simulate close particle interactions [52] by using a Monte Carlo binary collision model and is benchmarked to describe the dynamics of the proton beam in warm dense matter [53]. It can be well

*dwu.phys@zju.edu.cn
†zhaoyongtao@xjtu.edu.cn

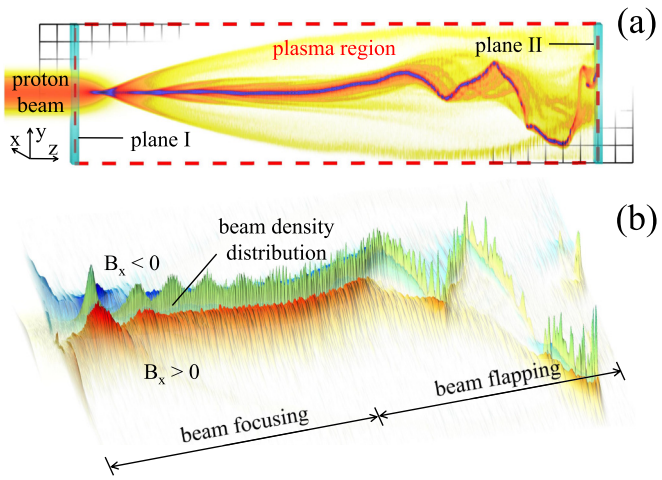

FIG. 1. (a) Schematic representation of the simulation model. Plasma is uniformly distributed within the red dashed box. Planes I and II are positions where the beam energy is measured. The black grids present the simulation cells. (b) Beam transport with the self-generated magnetic constraint. The red and blue surfaces stand for the self-generated magnetic fields in the x direction which are positive and negative, respectively. The green surface is the beam density distribution.

adapted for systems in which plasma electrons can respond to electromagnetic field changes in no time and their inertia can be accordingly neglected. Moreover, compared with the standard PIC code, this code is more time-saving and can avoid numerical instabilities [52,56], especially in the case of intense proton beams, because it calculates the electric field with Ohm's law while neglecting the electron inertia. LAPINS also has its advantages in ionization dynamics calculations [54] and laser-plasma interactions [55]. With this method, it is now possible to reveal the untouched phenomena in large-scale beam-plasma interactions with density differences by magnitudes.

Here the transport of continuous proton beams in plasmas with a density of 10^{18} cm^{-3} and size of 8 cm is simulated by the LAPINS code [52–56] for over 10 ns. In the simulations, the densities of injected proton beams vary from 10^{14} to 10^{16} cm^{-3} and the beam energies range from 0.4 to 4.0 MeV. Plasma gas cells and continuous proton beams with similar parameters are nowadays widely available. Hence, in principle, the simulation predictions can be confirmed by experiments. In this paper we report that the focusing and flapping of slab proton beams transporting in large-scale plasmas are closely related to self-generated magnetic fields. The analyses of the spatial growth rate of magnetic energy and energy deposition of the beams indicate that such behaviors are determined by the injected beam densities and energies. Moreover, we point out that the flapping of beams can cause remarkable nonlinear energy loss.

II. SIMULATION SETTINGS AND RESULTS

The system setup is displayed in Fig. 1(a). Here hydrogen plasma with a density of 10^{18} cm^{-3} and temperature of 4 eV is uniformly distributed in an area 8 cm long in the z direction and 4 mm along y. A continuous slab proton beam with a width of 0.8 mm (Gaussian distribution) is injected into the plasma along the z axis. For two-dimensional simulations, there are 2250 grids in the z direction and 100 grids in the y direction. The time step is 67 fs. Absorbing boundary conditions are imposed on the particles and fields in the z direction, while in the y direction periodic boundary conditions for plasma particles are applied instead. Two diagnostic planes marked I and II are used to measure particle energies. Figure 1(b) shows that the beam transport is significantly connected to the self-generated magnetic fields. Further simulation and analysis indicate that such magnetic fields are produced by the movement of collisional plasmas.

We scanned the injected proton beams with a fixed energy of 0.4 MeV and varying densities from 10^{14} to 10^{16} cm^{-3}. Figure 2 displays maps of proton beam densities n_b and magnetic fields B_x at 12 ns. When the beam density is 10^{14} cm^{-3} [Fig. 2(a)], the transport of protons in plasmas is quite ordinary. The beam is straightforward and only slightly deflected at the front end by collisions with background plasmas. For such a large density difference between injected proton beams and background plasmas, the collective electromagnetic field can hardly be generated. As shown in Fig. 2(b), the magnetic field is even weaker than the background fluctuations. Further simulations confirm that when the proton beam density is lower than 10^{14} m^{-3}, the collective effect of the plasma on the proton beam is not of any significance.

Figures 2(c) and 2(e) show obvious beam focusing when the beam density increases to 1×10^{15} and 5×10^{15} cm^{-3}, respectively. Similar beam focusing has been reported in beam-driven plasma wake-field acceleration studies [15–17] and plasma lens research [23–28]. Unlike the groups of focused ions moving along with the beam in a plasma wake field, here the focusing positions are almost fixed. Increasing the beam densities can intensify the focusing effect and shorten the distance between focusing positions. In Figs. 2(d) and 2(f), the self-generated magnetic field, as a result of the beam current and neutralizing current in collision plasmas, is obviously stronger than the background fluctuation. This simulation result, which indicates several beam self-focusing points with transverse width being reduced from 0.8 mm to 0.2 mm, is a great illustration of the beam self-focusing effect and agrees well with previous experiments [21,23] and analyses [25]. In Ref. [21] a plasma lens designed for the heavy-ion accelerator was investigated experimentally. The plasma pinch dynamics images showed multiple focusing points and similar particle distribution. In addition, a transverse beam size change from 6 mm to 2 mm was observed in overfocusing experiments on the neutralized drift compression experiment device in Ref. [23].

When the proton beam density reaches 5×10^{15} and 1×10^{16} cm^{-3}, as shown in Figs. 2(e) and 2(g), respectively, it is worth noting that the beam distribution in the high-z region undergoes another change apart from beam focusing. The transport path of the beam is no longer a straight line along the axis, but a curved path around it. The beam can flap like turbulence and may even totally deviate from the axis at the high-z region. So do the magnetic fields in Figs. 2(f) and 2(h). There have been studies [57,58] where particles undergo kinking, but hardly any of them have a parameter regime close

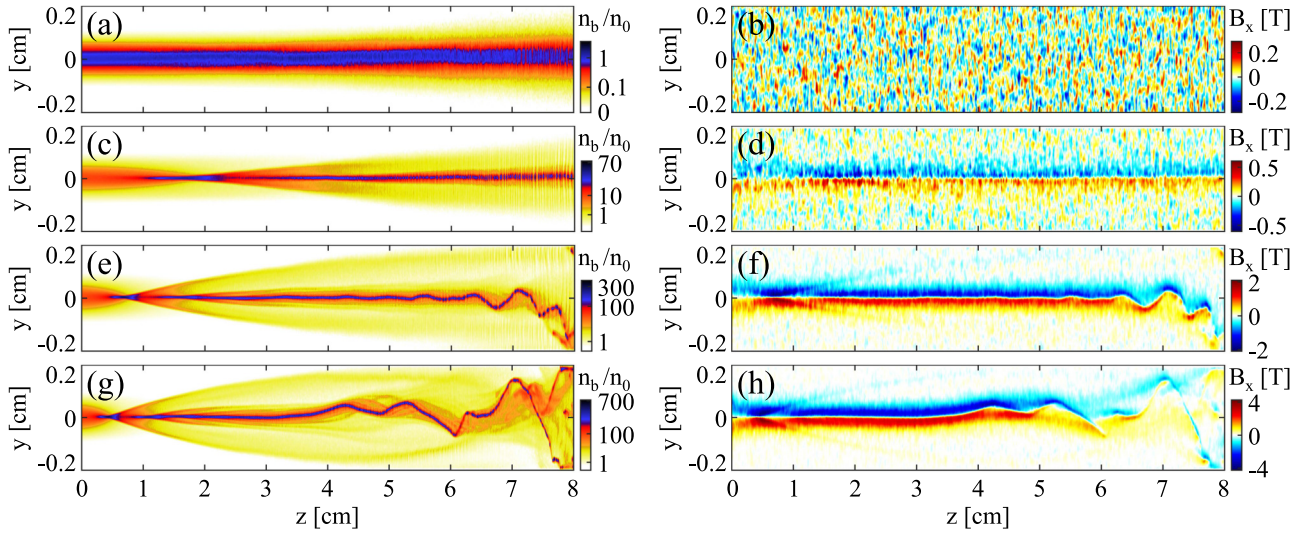

FIG. 2. Distributions of beam densities and magnetic fields for proton beams with different densities at 12 ns. The beam distributions (in units of $n_0 = 10^{14}$ cm^{-3}) have an injection energy of 0.4 MeV; initial densities of (a) 1×10^{14}, (c) 1×10^{15}, (e) 5×10^{15}, and (g) 1×10^{16} cm^{-3}; and current densities of (a) 1.4×10^{8}, (c) 1.4×10^{9}, (e) 7×10^{9}, and (g) 1.4×10^{10} A/m^2. The corresponding magnetic fields are shown in (b), (d), (f), and (h).

to ours. Our flapping result should be studied further in future works.

III. ANALYSIS AND DISCUSSION

In Cartesian coordinates (x, y, z), the Lorentz force acting on the beam protons can be expressed as

$$\begin{aligned} \boldsymbol{F}_b &= Z_b e\left(\boldsymbol{E} + \frac{\boldsymbol{v}_b}{c} \times \boldsymbol{B}\right) \\ &= Z_b e\left[\left(E_y + B_x \frac{v_b}{c}\right)\boldsymbol{e}_y + E_z \boldsymbol{e}_z\right], \end{aligned} \tag{1}$$

where the beam particle charge Z_b is 1, $\boldsymbol{v}_b$ is the beam velocity, c is the light speed, and the electric field and magnetic field are written as $\boldsymbol{E} = E_y \boldsymbol{e}_y + E_z \boldsymbol{e}_z$ and $\boldsymbol{B} = B_x \boldsymbol{e}_x$, respectively. Considering the system is time dependent, we express all quantities in coordinates (x, y, ξ), where $\xi = z - v_b t$. In the simulation, all particles are totally free in space. However, in this analysis, we assume that the plasma ions are fixed and the electron velocity is in the z direction, i.e., $\boldsymbol{v}_i = 0$ and $\boldsymbol{v}_e = v_{ez} \boldsymbol{e}_z$ for simplicity. The electron momentum equation becomes

$$(v_{ez} - v_b)\frac{\partial \boldsymbol{v}_e}{\partial \xi} = -\frac{e}{m_e}\left(\boldsymbol{E} + \frac{\boldsymbol{v}_e}{c} \times \boldsymbol{B}\right). \tag{2}$$

Here we make use of $d\boldsymbol{v}_e/dt = (v_{ez} - v_b)(\partial \boldsymbol{v}_e/\partial \xi) + v_{ey}(\partial \boldsymbol{v}_e/\partial y)$ and $v_{ey} = 0$. The y and z components of Eq. (2) yield

$$E_y = -\frac{B_x v_{ez}}{c}, \tag{3}$$

$$E_z = \frac{m_e}{e}(v_b - v_{ez})\frac{\partial v_{ez}}{\partial \xi}. \tag{4}$$

Making use of Faraday's law $\partial E_z/\partial y - \partial E_y/\partial \xi = v_b/c(\partial B_x/\partial \xi)$, we obtain

$$B_x = \frac{m_e c}{e}\frac{\partial v_{ez}}{\partial y}, \tag{5}$$

$$E_y = -\frac{m_e}{e} v_{ez}\frac{\partial v_{ez}}{\partial y}. \tag{6}$$

Substituting Eqs. (4)–(6) into Eq. (1) gives us the Lorentz force acting on the beam protons

$$\begin{aligned} \boldsymbol{F}_b &= \boldsymbol{F}_{by} + \boldsymbol{F}_{bz} \\ &= Z_b m_e (v_b - v_{ez})\left(\frac{\partial v_{ez}}{\partial y}\boldsymbol{e}_y + \frac{\partial v_{ez}}{\partial \xi}\boldsymbol{e}_z\right) \\ &= Z_b^2 m_e v_b (v_b - v_{ez})\frac{1}{n_e}\left(\frac{\partial n_b}{\partial y}\boldsymbol{e}_y + \frac{\partial n_b}{\partial \xi}\boldsymbol{e}_z\right). \end{aligned} \tag{7}$$

Here $\boldsymbol{F}_{by}$ and $\boldsymbol{F}_{bz}$ are the y and z components of $\boldsymbol{F}_b$. Considering that the proton beam is well neutralized, $n_e v_{ez} = Z_b n_b v_b$, and the plasma density is much larger than the beam density $n_e \gg n_b$, $\boldsymbol{F}_b$ can be simplified to

$$\boldsymbol{F}_b \approx \frac{Z_b^2 m_e v_b^2}{n_e}\left(\frac{\partial n_b}{\partial y}\boldsymbol{e}_y + \frac{\partial n_b}{\partial \xi}\boldsymbol{e}_z\right). \tag{8}$$

The same expression of $\boldsymbol{F}_{by}$ was derived in Refs. [25,59,60] where azimuthally symmetric beams were analyzed in cylindrical coordinates. On the one hand, $\boldsymbol{F}_{by}$ provides a strong focusing force at the low-z region when the beam density gradient in the y direction is large enough with a highly symmetrical distribution. On the other hand, as the beam transports, perturbations develop and can even cause a transverse displacement of the beam and $\boldsymbol{F}_{by}$ will deflect the beam further in this case.

In our simulation, the initial perturbations actually result from the collision and get boosted by the magnetic field. According to Ref. [52], the beam current $\boldsymbol{J}_b$ and magnetic field $\boldsymbol{B}$ are connected by Ohm's law $\boldsymbol{E} + (\boldsymbol{v}_e/c) \times \boldsymbol{B} = \eta \boldsymbol{J}_b$ and Faraday's law $\partial \boldsymbol{B}/\partial t = -c\nabla \times \boldsymbol{E}$ in cgs units, where η is the resistivity. Resistivity η can be calculated with an empirical formula in usual hybrid PIC simulations where the plasma is treated as a fluid. However, we have a natural method to model

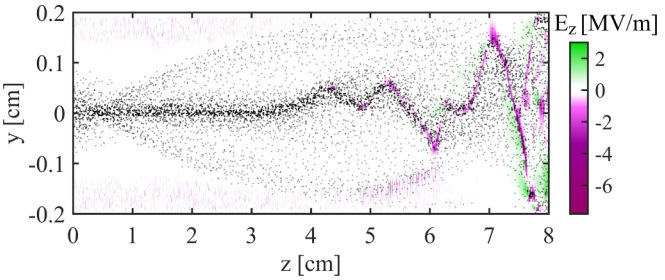

FIG. 3. The z component of the electric field with a beam density of 1×10^{16} cm^{-3} at 12 ns. Other conditions are the same as in Fig. 2(g). The black dots reveal the distribution of beam particles.

resistivity in our simulation by using the Monte Carlo binary collision model. This model was benchmarked in Ref. [53], where the stopping power of protons in solid-state aluminum was studied. Here resistivity η is calculated by averaging over all binary collisions at each time step for each simulation cell. For low electron velocity, we have $\boldsymbol{B} = -\int c\nabla \times (\eta \boldsymbol{J}_b)dt$. When the beam density is 10^{14} cm^{-3} in Fig. 2(b), the magnetic field is basically a background noise, which is around 0.2 T. In contrast, it can be as large as 2 T when the beam density is 5×10^{15} cm^{-3}, as shown in Fig. 2(f). The transverse magnetic pressure on the proton beam will increase by 100 times.

While the magnetic field makes a great contribution to $\boldsymbol{F}_{by}$, the electric field is the main cause of the damping force $\boldsymbol{F}_{bz}$. Figure 3 displays the electric field in the z direction at 12 ns when the beam density is 1×10^{16} cm^{-3}. Other conditions are the same as those in Fig. 2(g). The z component of the electric field is very small before $z = 4$ cm, but can reach several megavolts per meter where the beam flaps and gets scattered.

To study the focusing and flapping, we evaluate the spatial growth rate over a transport distance of 8 cm by analyzing the magnetic field energy, which is $E_{B_x} = \sum (B_x^2/8\pi)\delta x \delta y \delta z$ in our case. Here the summation domain is the whole simulation area (8 cm × 4 mm). It can be related to the spatial growth rate γ when written as $E_{B_x} \sim E_0 \exp(\gamma z)$, where z is the transport distance and E_0 is the initial magnetic energy.

The magnetic field energies E_{B_x} and corresponding spatial growth rates γ for fixed 0.4-MeV beams with different densities as a function of distance are displayed in Fig. 4(a). Generally, it takes 10 ns for these beams to reach $z = 8$ cm. The logarithmic energy increases sharply at early stage and then is followed by a saturation stage. We find that the magnetic energy in the case of a higher-density beam rises faster. Figure 4(b) presents the spatial growth rates as the derivatives of curves in Fig. 4(a). The growth rate of the higher beam density is generally larger.

We also analyze the influence of the injected beam energy on the magnetic field energy and spatial growth rate in Figs. 4(c) and 4(d), where the beam density is fixed at 10^{16} cm^{-3} and the energy varies from 0.4 to 0.8 to 1.6 to 4.0 MeV. The time spent getting $z = 8$ cm is around 10, 7, 5, and 3 ns, respectively. A high-energy beam can cause high magnetic field energy, while the spatial growth rate also increases. The development of high-energy beams is faster than that of low-energy beams at the early stage.

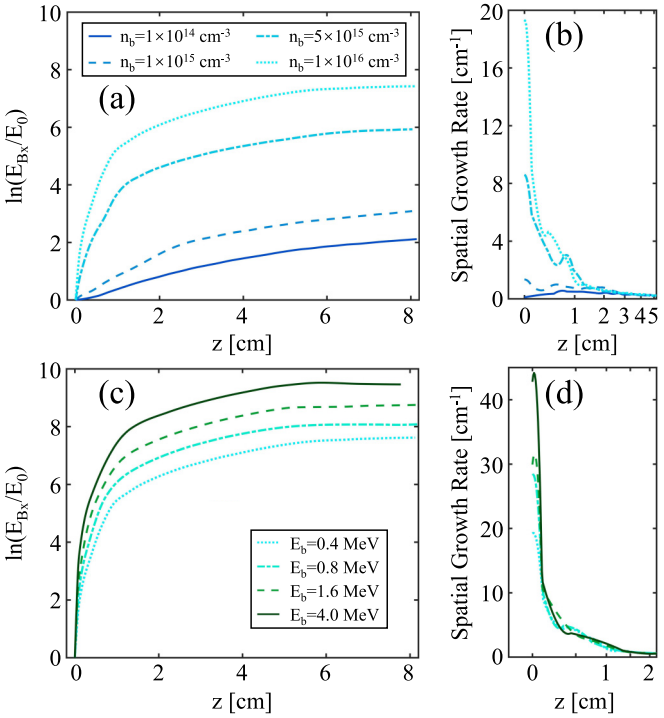

FIG. 4. Evolution as a function of distance: (a) magnetic field energies and (b) spatial growth rates for proton beams with a fixed initial energy of 0.4 MeV but different densities, and (c) magnetic field energies and (d) spatial growth rates for a proton beam with a fixed density of 10^{16} cm^{-3} but different initial energies.

Additionally, the focusing and flapping of beams have an obvious impact on beam energy deposition, which results from a longer transport path and the damping force $\boldsymbol{F}_{bz}$ caused by the electric field. Figure 5 shows the beam spectra with densities of 10^{14}, 10^{15}, 5×10^{15}, and 10^{16} cm^{-3} measured on plane II at 13.33 ns. They have the same initial spectrum of 0.4 MeV, which is detected on plane I. More details are presented in Table I. When the beam density is 10^{14} cm^{-3}, there is hardly any focusing and the energy loss is 50 keV in the simulation. According to Bethe's theory [61,62], for a single particle with speed $v \ll c$, charge Z, and energy E, its

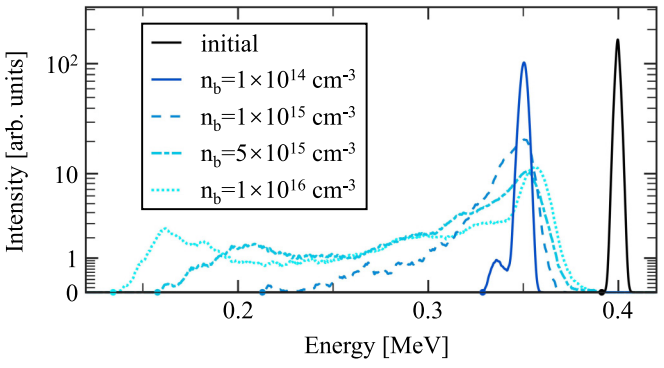

FIG. 5. Beam energy spectra for different densities measured on plane II at 13.33 ns. The black curve is the initial spectrum of these beams, detected on plane I. The dots at the bottom are the minimum energies detected.

TABLE I. Beam density (BD), average energy (AE), minimum energy (ME), and energy loss percentage (ELP) after passing through plasmas for four simulation cases with different densities.

Parameters	Case 1	Case 2	Case 3	Case 4
BD (cm^{-3})	1×10^{14}	1×10^{15}	5×10^{15}	1×10^{16}
AE (keV)	350	337	307	296
ME (keV)	330	215	160	139
ELP	12.5%	15.8%	23.3%	26.0%

energy loss per unit distance when being transported through a plasma of density n_p and frequency $\omega_p = (4\pi n_p e^2/m_e)^{1/2}$ reads, in cgs units, $-dE/dz = (Z^2 e^2 \omega_p^2/v^2)\ln(2m_e v^2/\hbar\omega_p)$. Thus, the theoretical total energy loss of a single proton in our condition is 6.02 keV/cm × 8 cm = 48.16 keV. The theoretical result agrees well with our simulation results even when the beam density is four orders of magnitude lower than the plasma density. However, when the beam density rises, focusing and flapping occur and the spectrum extends toward the lower-energy region. Both the average energy and minimum energy decrease. As the beam density increases from 10^{14} cm^{-3} to 10^{16} cm^{-3}, the energy loss percentage climbs from 12.5% to 26.0% and the minimum energy of the beam particles drops from 330 keV to 139 keV, which is obviously nonlinear. Further studies are still necessary to validate these quantitative results.

Considering the results in Fig. 2, our simulation reveals evident beam focusing when the beam density is higher than 10^{15} cm^{-3} and there is a small average energy difference of 15 keV compared with Bethe's theory. Moreover, the beam can curve and flap when the beam density is higher than 10^{16} cm^{-3}. The beam travels a path longer than the actual plasma size like turbulence with the influence of a damping force. Particles detected by plane II can lose 65% of their initial energies at most. The remarkable nonlinear energy loss increase we observed is of great importance in ICF [7,8] and high-energy density physics [3–6].

IV. CONCLUSION

In summary, the transport for continuous intense slab proton beams through hydrogen plasmas with a density of 10^{18} cm^{-3} and size of 8 cm was simulated by the LAPINS PIC code for over 10 ns. The focusing and flapping of the beam were observed and studied. In the simulation, the prominent beam self-focusing effect agreed well with previous theory. When the beam density increased, the beam could curve and flap like turbulence. Simulation and analysis indicated that the self-generated magnetic fields, produced by the movement of collisional plasmas, play an important role in focusing and deflecting the beams. In the analysis of the spatial growth rate of magnetic energy and beam energy deposition, beam focusing and flapping were found to be related to the beam densities and energies. A higher beam density could cause an obvious increase of the magnetic field energy. We pointed out that such beam behaviors can cause remarkable nonlinear energy loss. Our simulations provide clear pictures for the transport and energy deposition of very intense ion beams in plasmas, but await quantitative validation through further independent simulation studies. The results might find innovative applications in fusion sciences and astrophysics and could also be of interest for the focusing, modulating, or dumping of intense ion beams at large-scale accelerators.

ACKNOWLEDGMENTS

This work was supported by National Key R&D Program of China (Grant No. 2019YFA0404900), Science Challenge Project (Grant No. TZ2016005), National Natural Science Foundation of China (Grants No. 11705141, No. 11605269, No. 11775282, and No. U1532263), and China Postdoctoral Science Foundation (Grants No. 2017M623145 and No. 2018M643613).

[1] A. Martinez de la Ossa, T. J. Mehrling, and J. Osterhoff, Phys. Rev. Lett. **121**, 064803 (2018).
[2] M. Litos, E. Adli, W. An, C. I. Clarke, C. E. Clayton, S. Corde, J. P. Delahaye, R. J. England, A. S. Fisher, J. Frederico *et al.*, Nature (London) **515**, 92 (2014).
[3] N. A. Tahir, F. Burkart, A. Shutov, R. Schmidt, D. Wollmann, and A. R. Piriz, Phys. Rev. E **90**, 063112 (2014).
[4] L. Zhang, Y. Zhao, J. Ren, D. Wu, W. Liu, G. Feng, W. Ma, R. Cheng, G. Xiao, D. H. H. Hoffmann, and Z. Xu, Phys. Plasmas **25**, 113108 (2018).
[5] J. Ren, Y. Zhao, L. Bozyk, C. Maurer, A. Blazevic, P. Spiller, G. Xiao, and D. H. H. Hoffmann, Nucl. Instrum. Methods Phys. Res. Sect. B **429**, 48 (2018).
[6] B. Y. Sharkov, D. H. H. Hoffmann, A. A. Golubev, and Y. Zhao, Matter Radiat. Extremes **1**, 28 (2016).
[7] R. K. Follett, J. A. Delettrez, D. H. Edgell, V. N. Goncharov, R. J. Henchen, J. Katz, D. T. Michel, J. F. Myatt, J. Shaw, A. A. Solodov, C. Stoeckl, B. Yaakobi, and D. H. Froula, Phys. Rev. Lett. **116**, 155002 (2016).
[8] T. Kubo, T. Karino, H. Kato, and S. Kawata, IEEE Trans. Plasma Sci. **47**, 2 (2019).
[9] A. Spitkovsky, Astrophys. J. Lett. **673**, L39 (2008).
[10] C. M. Huntington, F. Fiuza, J. S. Ross, A. B. Zylstra, R. P. Drake, D. H. Froula, G. Gregori, N. L. Kugland, C. C. Kuranz, M. C. Levy *et al.*, Nat. Phys. **11**, 173 (2015).
[11] V. N. Zirakashvili, V. S. Ptuskin, and H. J. Voelk, Astrophys. J. **678**, 255 (2008).
[12] A. Spitkovsky, Astrophys. J. Lett. **682**, L5 (2008).
[13] A. P. L. Robinson, D. J. Strozzi, J. R. Davies, L. Gremillet, J. J. Honrubia, T. Johzaki, R. J. Kingham, M. Sherlock, and A. A. Solodov, Nucl. Fusion **54**, 054003 (2014).
[14] E. Adli, A. Ahuja, O. Apsimon, R. Apsimon, A. M. Bachmann, D. Barrientos, F. Batsch, J. Bauche, V. K. B. Olsen, M. Bernardini *et al.*, Nature (London) **561**, 363 (2018).
[15] A. Caldwell, K. Lotov, A. Pukhov, and F. Simon, Nat. Phys. **5**, 363 (2009).
[16] M. Turner, E. Adli, A. Ahuja, O. Apsimon, R. Apsimon, A. M. Bachmann, M. B. Marin, D. Barrientos, F. Batsch, J. Batkiewicz *et al.*, Phys. Rev. Lett. **122**, 054801 (2019).

[17] E. Adli, A. Ahuja, O. Apsimon, R. Apsimon, A. M. Bachmann, D. Barrientos, M. M. Barros, J. Batkiewicz, F. Batsch, J. Bauche *et al.*, Phys. Rev. Lett. **122**, 054802 (2019).
[18] W. Panofsky and W. Baker, Rev. Sci. Instrum. **21**, 445 (1950).
[19] E. Boggasch, J. Jacoby, H. Wahl, K.-G. Dietrich, D. H. H. Hoffmann, W. Laux, M. Elfers, C. R. Haas, V. P. Dubenkov, and A. A. Golubev, Phys. Rev. Lett. **66**, 1705 (1991).
[20] D. Hoffmann, R. Bock, A. Faenov, U. Funk, M. Geissel, U. Neuner, T. Pikuz, F. Rosmej, M. Roth, W. Suss, N. Tahir, and A. Tauschwitz, Nucl. Instrum. Methods Phys. Res. Sect. B **161**, 9 (2000).
[21] M. Basko, A. Drozdovskii, A. Golubev, K. Gubskii, D. Iosseliani, A. Kantsyrev, M. Karpov, A. Kuznetsov, Y. Novozhilov, O. Pronin, S. Savin, P. Sasorov, D. Sobur, B. Sharkov, and V. Yanenko, Phys. Part. Nuclei Lett. **5**, 582 (2008).
[22] M. Chabot, D. Gardes, P. Box, J. Kiener, C. Deutsch, G. Maynard, V. Andre, C. Fleurier, D. Hong, and K. Wohrer, Phys. Rev. E **51**, 3504 (1995).
[23] A. B. Sefkow, R. C. Davidson, E. P. Gilson, I. D. Kaganovich, A. Anders, J. E. Coleman, M. Leitner, S. Lidia, P. K. Roy, and P. A. Seidl, Phys. Plasmas **16**, 234801 (2009).
[24] P. A. Seidl, A. Anders, F. M. Bieniosek, J. J. Barnard, J. Calanog, A. X. Chen, R. H. Cohen, J. E. Coleman, M. Dorf, E. P. Gilson, D. P. Grote, J. Y. Jung, M. Leitner, S. M. Lidia, B. G. Logan, P. Ni, P. K. Roy, K. Van den Bogert, W. L. Waldron, and D. R. Welch, Nucl. Instrum. Methods Phys. Res. Sect. A **606**, 75 (2009).
[25] I. D. Kaganovich, R. C. Davidson, M. A. Dorf, E. A. Startsev, A. B. Sefkow, E. P. Lee, and A. Friedman, Phys. Plasmas **17**, 056703 (2010).
[26] M. A. Dorf, I. D. Kaganovich, E. A. Startsev, and R. C. Davidson, Phys. Plasmas **18**, 033106 (2011).
[27] R. C. Davidson, M. A. Dorf, I. D. Kaganovich, H. Qin, A. Sefkow, E. A. Startsev, D. R. Welch, D. V. Rose, and S. M. Lund, Nucl. Instrum. Methods Phys. Res. Sect. A **606**, 11 (2009).
[28] H. Uhm, R. Davidson, and I. Kaganovich, Phys. Plasmas **8**, 4637 (2001).
[29] Z. H. Hu, X. J. Wang, Y. T. Zhao, and Y. N. Wang, Phys. Plasmas **24**, 123103 (2017).
[30] N. Liu, Z. Wang, M. Sun, R. Deiterding, and H. Wang, Aerosp. Sci. Technol. **91**, 456 (2019).
[31] D. Martinez-Ruiz, C. Huete, P. J. Martinez-Ferrer, and D. Mira, J. Fluid Mech. **872**, 889 (2019).
[32] R. Yan, A. V. Maximov, C. Ren, and F. S. Tsung, Phys. Rev. Lett. **103**, 175002 (2009).
[33] D. J. Economou, Plasma Process. Polym. **14**, 1600152 (2017).
[34] S. Markidis, P. Henri, G. Lapenta, K. Ronnmark, M. Hamrin, Z. Meliani, and E. Laure, J. Comput. Phys. **271**, 415 (2014).
[35] H. Fahr, T. Kausch, and H. Scherer, Astron. Astrophys. **357**, 268 (2000).
[36] F. Valentini, P. Travnciek, F. Califano, P. Hellinger, and A. Mangeney, J. Comput. Phys. **225**, 753 (2007).
[37] T. D. Arber, K. Bennett, C. S. Brady, A. Lawrence-Douglas, M. G. Ramsay, N. J. Sircombe, P. Gillies, R. G. Evans, H. Schmitz, A. R. Bell, and C. P. Ridgers, Plasma Phys. Controlled Fusion **57**, 113001 (2015).
[38] D. Wu, W. Yu, Y. T. Zhao, S. Fritzsche, and X. T. He, Matter Radiat. Extremes **3**, 293 (2018).
[39] J. Kim, B. Qiao, C. McGuffey, M. S. Wei, P. E. Grabowski, and F. N. Beg, Phys. Rev. Lett. **115**, 054801 (2015).
[40] J. Teunissen and U. Ebert, Plasma Sources Sci. Technol. **25**, 044005 (2016).
[41] M. A. Riquelme, E. Quataert, and D. Verscharen, Astrophys. J. **824**, 123 (2016).
[42] L. Collins, I. Kwon, J. Kress, N. Troullier, and D. Lynch, Phys. Rev. E **52**, 6202 (1995).
[43] P. E. Grabowski, M. P. Surh, D. F. Richards, F. R. Graziani, and M. S. Murillo, Phys. Rev. Lett. **111**, 215002 (2013).
[44] C. E. Torres, H. Parishani, O. Ayala, L. F. Rossi, and L. P. Wang, J. Comput. Phys. **245**, 235 (2013).
[45] G. L. Bryan and the Enzo Collaboration, Astrophys. J. Suppl. Ser. **211**, 19 (2014).
[46] G. Rein, Math. Meth. Appl. Sci. **17**, 1129 (1994).
[47] G. Joyce, G. Knorr, and H. K. Meier, J. Comput. Phys. **8**, 53 (1971).
[48] E. M. Epperlein, G. J. Rickard, and A. R. Bell, Comput. Phys. Commun. **52**, 7 (1988).
[49] L. Sironi and A. Spitkovsky, Astrophys. J. Lett. **707**, L92 (2009).
[50] C. B. Schroeder, C. Benedetti, E. Esarey, F. J. Grüner, and W. P. Leemans, Phys. Rev. E **86**, 026402 (2012).
[51] M. Roth, T. E. Cowan, M. H. Key, S. P. Hatchett, C. Brown, W. Fountain, J. Johnson, D. M. Pennington, R. A. Snavely, S. C. Wilks, K. Yasuike, H. Ruhl, P. Pegoraro, S. V. Bulanov, E. M. Campbell, M. D. Perry, and H. Powell, Phys. Rev. Lett. **86**, 436 (2001).
[52] D. Wu, W. Yu, Y. T. Zhao, D. H. H. Hoffmann, S. Fritzsche, and X. T. He, Phys. Rev. E **100**, 013208 (2019).
[53] D. Wu, X. T. He, W. Yu, and S. Fritzsche, Phys. Rev. E **95**, 023207 (2017).
[54] D. Wu, X. T. He, W. Yu, and S. Fritzsche, Phys. Rev. E **95**, 023208 (2017).
[55] D. Wu, X. T. He, W. Yu, and S. Fritzsche, High Power Laser Sci. Eng. **6**, e50 (2018).
[56] D. Wu, W. Yu, S. Fritzsche, and X. T. He, Phys. Rev. E **100**, 013207 (2019).
[57] S. C. Hsu and P. M. Bellan, Phys. Rev. Lett. **90**, 215002 (2003).
[58] M. V. Barkov and S. S. Komissarov, Mon. Not. R. Astron. Soc. **458**, 1939 (2016).
[59] M. A. Dorf, I. D. Kaganovich, E. A. Startsev, and R. C. Davidson, Phys. Rev. Lett. **103**, 075003 (2009).
[60] K. Hahn and E. Lee, Fusion Eng. Des. **32**, 417 (1996).
[61] H. Bethe, Ann. Phys. (Leipzig) **5**, 325 (1930).
[62] H. Bethe, Z. Phys. **76**, 293 (1932).